Dipole strength distribution in ^{56}Fe

T. Shizuma,[1] T. Hayakawa,[1] H. Ohgaki,[2] H. Toyokawa,[3] T. Komatsubara,[4] N. Kikuzawa,[5] T. Inakura,[6,7] M. Honma,[8] and H. Nakada[7]

[1]*Quantum Beam Science Directorate, Japan Atomic Energy Agency, Tokai, Ibaraki 319-1195, Japan*
[2]*Institute of Advanced Energy, Kyoto University, Uji, Kyoto 611-0011, Japan*
[3]*National Institute of Advanced Industrial Science and Technology, Tsukuba, Ibaraki 305-8568, Japan*
[4]*Institute of Physics, University of Tsukuba, Tsukuba, Ibaraki 305-8571, Japan*
[5]*J-PARC Center, Japan Atomic Energy Agency, Tokai, Ibaraki 319-1195, Japan*
[6]*Theoretical Nuclear Physics Laboratory, RIKEN Nishina Center, Wako, Saitama 351-0198, Japan*
[7]*Department of Physics, Graduate School of Science, Chiba University, Inage, Chiba 263-8522, Japan*
[8]*Center for Mathematical Sciences, University of Aizu, Aizu-Wakamatsu, Fukushima 965-8580, Japan*

(Received 1 March 2012; revised manuscript received 27 December 2012; published 4 February 2013)

Electromagnetic dipole transitions in ^{56}Fe were measured in photon-scattering experiments with a linearly polarized photon beam. The parity quantum numbers of the excited dipole states were determined by the intensity asymmetry of resonantly scattered γ rays with respect to the polarization plane of the incident photon beam. While the summed magnetic dipole ($M1$) strength was determined as $\Sigma B(M1)\uparrow = 3.52(17)\ \mu_N^2$ at excitation energies between 7 and 10 MeV, the summed electric dipole ($E1$) strength below 10 MeV was obtained as $\Sigma B(E1)\uparrow = 78.0(15) \times 10^{-3}\ e^2\ \mathrm{fm}^2$. The observed $M1$ strength was compared with shell-model predictions in the pf shell using the GXPF1J and KB3G effective interactions. In addition, the $E1$ strength was compared with random-phase approximation calculations with the Skyrme interaction.

DOI: 10.1103/PhysRevC.87.024301 PACS number(s): 25.20.Dc, 23.20.−g, 21.10.Hw, 27.40.+z

I. INTRODUCTION

Magnetic dipole ($M1$) response is one of the fundamental characteristics of atomic nuclei. The nucleon spin interacts with the nuclear magnetic current through the electromagnetic field. Therefore, the $M1$ response provides direct information on the spin-dependent part of the nuclear interaction [1], which is of particular importance for the estimation of inelastic neutrino-nucleus cross sections relevant to core-collapse supernova explosions [2].

Nuclei with $A \sim 56$ in the vicinity of the closed $N = Z = 28$ shells exhibit one of the most favorable regions for observing a spin-flip $M1$ resonance. In the independent-particle model [3], a strong spin-flip $M1$ transition in these nuclei can be interpreted in terms of both proton and neutron $1f_{7/2}^{-1}1f_{5/2}$ particle-hole excitations. The nucleus ^{56}Fe lies in this region and differs from the doubly magic nucleus ^{56}Ni by four nucleons, having two protons fewer and two neutrons more, i.e., $\pi 1f_{7/2}^{-2} \otimes \nu 2p_{3/2}^{2}$. The energy gap between the $1f_{7/2}$-$1f_{5/2}$ spin-orbit pair is about 6 MeV [3]. Therefore, a substantial $M1$ strength of the $1f_{7/2}^{-1}1f_{5/2}$ particle-hole excitation can be expected in this energy region. However, in inelastic electron-scattering measurements [4–6], $M1$ strengths associated with this particle-hole excitation have been observed in the region of excitation energies E_x between 7 and 10 MeV. The difference between the expected and the observed excitation energies can be explained by the repulsive nature of the residual interaction relevant to the isovector $M1$ excitation.

The electric dipole ($E1$) response at energies around the particle separation energy is also attracting increasing attention in nuclear structure physics [7] as well as nuclear astrophysics [8]. The concentration of the $E1$ strength around the particle separation energy is commonly termed the pygmy dipole resonance (PDR) because of its weak strength in comparison with the giant dipole resonance (GDR), which dominates the $E1$ strength in nuclei. Because the PDR strength is correlated to neutron skin thickness [9], which is related to the equation of state (EOS) of the neutron-rich matter [10], investigation of the PDR may provide information on the properties of neutron stars, such as the proton ratio and radius. A concentration of low-energy $E1$ strength has been experimentally observed in both stable and unstable nuclei such as O [11,12], Ca [13], Ni [14], Sn [15–17], and Pb isotopes [18,19] as well as the $N = 82$ isotones [20–22]. The total sum of the measured energy-weighted strengths of such $E1$ concentrations is less than about 1% of the Thomas-Reiche-Kuhn (TRK) sum rule value for stable nuclei and less than 5% for unstable neutron-rich nuclei. For stable pf-shell nuclei, a relatively small low-energy $E1$ strength, less than 0.3% of the TRK sum rule value was observed in ^{56}Fe and ^{58}Ni [23].

Until now, the information on dipole excitations of ^{56}Fe has been obtained from nuclear resonance fluorescence (NRF) experiments using unpolarized or partially polarized bremsstrahlung [23–26]. Although the excitation energies and the ground-state decay width Γ_0 have been obtained for 53 dipole states of ^{56}Fe, parity quantum numbers have been determined for only 16 excited levels, including 8 positive party states at excitation energies below 10 MeV [23].

Because the NRF process occurs via the well-known electromagnetic interaction, the scattering cross sections, and the spin and parity quantum numbers of excited states can be extracted in a model-independent way [27]. Recently, it has been shown that a quasimonochromatic, linearly polarized photon beam produced by laser Compton scattering considerably increases experimental sensitivities, particularly for the determination of the parity quantum numbers of resonantly

excited states [28,29]. In this paper, we present results of a NRF experiment on ^{56}Fe. The $M1$ strength is investigated by using shell-model calculations with different types of effective interactions, i.e., GXPF1J [30,31] and KB3G [32], both of which are widely used for shell-model studies of pf-shell nuclei. The $E1$ strength distribution is compared with results obtained from random-phase approximation (RPA) calculations using the Skyrme functional of SkM* as well [33].

II. EXPERIMENTAL PROCEDURE

The present photon-scattering experiment was performed at the Tsukuba Electron Ring for Acceleration and Storage (TERAS) facility of the National Institute of Advanced Industrial Science and Technology (AIST) [34]. A quasimonochromatic, linearly polarized photon beam was generated by backward Compton scattering between laser light and high-energy electrons. A Nd:YVO_4 laser with a wavelength of 1064 nm at a frequency of 20 kHz was used. The electron energies were selected as 657, 698, and 755 MeV to produce quasimonochromatic photon beams with maximum energies $E_\gamma^{\max}$ of 7.6, 8.6, and 10.0 MeV, respectively. A 20-cm-thick lead collimator with a 4-mm aperture was used to form a quasimonochromatic photon beam with $\Delta E/E \approx 10\%$ at full width at half maximum (FWHM). The average intensity on the target was 3×10^5 photons/s, measured with a large-volume ($8'' \times 12''$) NaI(Tl) scintillation detector. The target consisted of a natural iron cylinder (91.8% ^{56}Fe) with an 11-mm diameter and a 31-mm length. It was surrounded by two high-purity Ge detectors with efficiencies of 120% and 140% relative to a $3'' \times 3''$ NaI scintillation detector. The Ge detectors were placed horizontally at a scattering angle of $\theta = \pm 90^\circ$. The typical energy resolution of the Ge detectors was $\Delta E_\gamma/E_\gamma \approx 0.09\%$ at FWHM at $E_\gamma \approx 7$ MeV. A 50-mm-thick lead collimator with a 40×20 mm^2 entrance window was placed in front of each Ge detector. To reduce background counts originating from bremsstrahlung due to high-energy electrons in the storage ring, events correlated within 1 μs of laser pulses were stored.

Figure 1 shows an energy spectrum of the incident photon beam measured by the Ge detector with a 120% relative efficiency. A Monte Carlo simulation was performed with

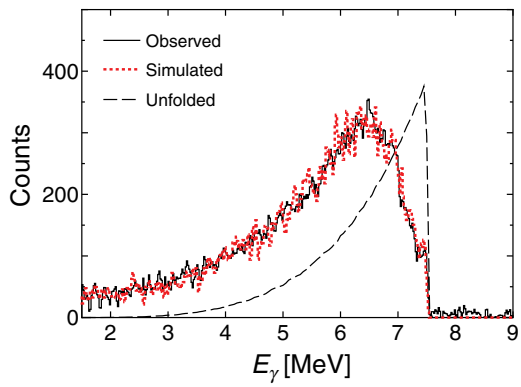

FIG. 1. (Color online) Energy spectrum of the incident photon beam measured with a Ge detector (solid line). The original incident photon spectrum shown with the dashed line was obtained by unfolding the simulated energy distribution (dotted line).

the ELECTRON GAMMA SHOWER (EGS) code [35] to analyze the response of the Ge detector. The energy distribution of the incident photon beam was extracted by unfolding the resulting simulated spectrum so as to reproduce the observed energy distribution.

The intensity asymmetry of the resonantly scattered photons with respect to the polarization plane of the incident photon beam serves as the basis for parity determination. The azimuthal angular distribution of dipole transitions can be expressed as

$$W(\theta, \phi) = W(\theta) \mp \tfrac{3}{4}(1 - \cos^2\theta)\cos\phi, \tag{1}$$

where θ is the scattering angle between the incoming and scattered photons and ϕ is the azimuthal angle defined by the polarization plane (formed by the propagation direction and the electric field vector of the incident photon beam) and the reaction plane. $W(\theta)$ is the angular correlation function for unpolarized radiation. A more general form of Eq. (1) can be found in the article by Fagg and Hanna [36].

The analyzing power for parity determination is defined [28] using the azimuthal angular distributions of $W(90^\circ, 0^\circ)$ and $W(90^\circ, 90^\circ)$ as

$$\Sigma = \frac{W(90^\circ, 0^\circ) - W(90^\circ, 90^\circ)}{W(90^\circ, 0^\circ) + W(90^\circ, 90^\circ)}. \tag{2}$$

Under the condition of complete polarization for the incoming photon beam, $\Sigma = +1$ is expected for $M1$ transitions, and $\Sigma = -1$ is expected for $E1$ transitions.

The corresponding intensity asymmetry of the observed NRF γ rays is given by

$$A = \frac{N_\parallel - N_\perp}{N_\parallel + N_\perp} = q\Sigma, \tag{3}$$

where $N_\parallel$ ($N_\perp$) represents the measured intensity of NRF γ rays detected at $\theta = \pm 90^\circ$ in the plane parallel (perpendicular) to the polarization plane. Here, q is the experimental sensitivity of the detection system, which is less than unity because of the finite solid angle of the Ge detectors and the spatially extended target. In the present case, q is estimated to be 0.85 from the numerical simulation [29]. Thus, on the basis of the azimuthal intensity asymmetry, the multipolarities of resonantly scattered transitions can be determined.

III. RESULTS

Figure 2 shows the photon-scattering spectra obtained at polar and azimuthal angles of $(\theta, \phi) = (90^\circ, 0^\circ)$ and $(90^\circ, 90^\circ)$ from the measurement with the maximum beam energy $E_\gamma^{\max} = 7.6$ MeV. Peaks shown with spin and parity quantum numbers represent ground-state transitions. We confirmed a total of 36 γ-ray transitions between 6.9 and 9.8 MeV. Several transitions with relatively small integrated cross sections reported in the previous work [23] could not be confirmed in the present experiment.

The parity of the excited states is given on the basis of the azimuthal intensity asymmetry from Eqs. (2) and (3). As shown in Fig. 3, the data are separated depending on their multipolarities ($E1$ or $M1$). The deviation from the

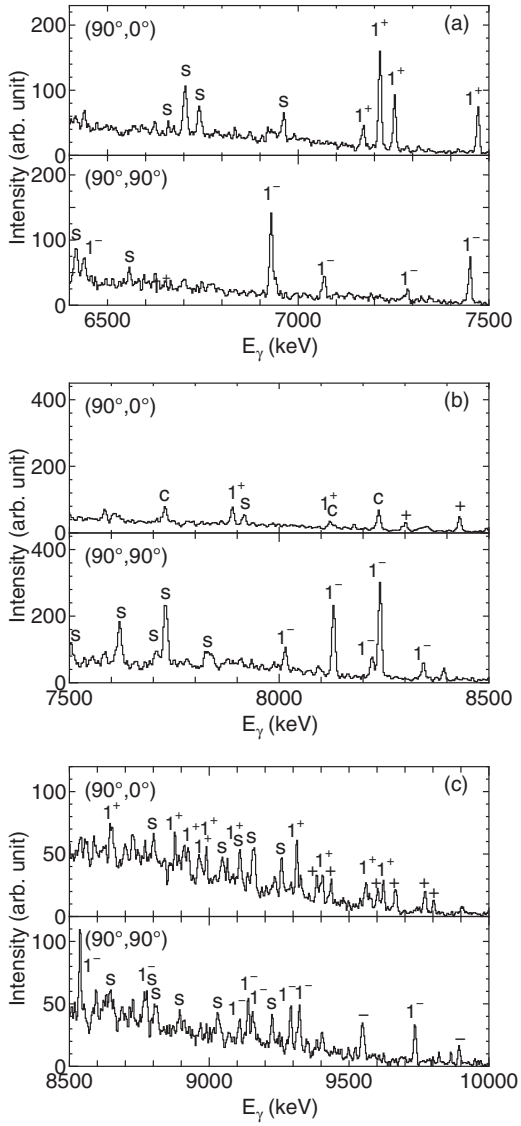

FIG. 2. Typical photon-scattering spectra observed at polar and azimuthal angles of $(\theta, \phi) = (90^\circ, 0^\circ)$ and $(90^\circ, 90^\circ)$ from the measurements with the maximum beam energy $E_\gamma^{\max}$ of (a) 7.6 MeV, (b) 8.6 MeV, and (c) 10.0 MeV. The J^π assignments are indicated for the ground-state transitions in ^{56}Fe. Peaks labeled c and s are due to contamination of the $E1$ transitions and single escapes, respectively.

expectation ($A = \pm 0.85$) is due to the proximity of the γ-ray peaks, especially in higher-energy transitions. As a result of the present measurement, the parity quantum numbers for 24 known and 4 unknown levels were newly determined, and parities opposite to those in Ref. [23] were assigned to the 7166.0 and 9107.8 keV levels.

The reduced transition probabilities were extracted from the ground-state decay width Γ_0 taken from Ref. [23], using the following relations:

$$B(E1)\uparrow = 2.866\frac{\Gamma_0}{E_\gamma^3}\ [10^{-3}e^2\ \mathrm{fm}^2], \tag{4}$$

$$B(M1)\uparrow = 0.2598\frac{\Gamma_0}{E_\gamma^3}\ [\mu_N^2], \tag{5}$$

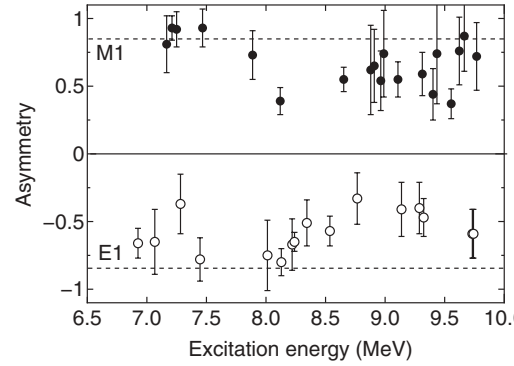

FIG. 3. Azimuthal intensity asymmetry obtained for $E1$ (open circles) and $M1$ (solid circles) transitions in ^{56}Fe. The experimental sensitivity q (=0.85) deduced from the numerical calculation is indicated by dashed lines.

where Γ_0 is given in meV and E_γ in MeV. The experimental results are summarized in Table I.

Among the dipole excitations in the $E_x = 6.9 \sim 9.8$ MeV region, 17 states were assigned to be 1^+ and 16 states were assigned to be 1^- from the present measurement using the polarized photon beam. The summed $M1$ strength in this energy region is obtained as $\Sigma B(M1)\uparrow = 3.52(17)\ \mu_N^2$, while the summed $E1$ strength is $\Sigma B(E1)\uparrow = 78.0(15) \times 10^{-3}\ e^2\ \mathrm{fm}^2$. If the transitions whose spin values are not determined are assumed to be of dipole character (9434.9, 9664.7, 9732.2, and 9768.2 keV), the summed $M1$ and $E1$ strengths increase to $\Sigma B(M1)\uparrow = 3.83(18)\ \mu_N^2$ and $\Sigma B(E1)\uparrow = 79.6(15) \times 10^{-3}\ e^2\ \mathrm{fm}^2$, respectively. These are greater than the values of $\Sigma B(M1)\uparrow = 1.37(12)\ \mu_N^2$ and $\Sigma B(E1)\uparrow = 60.2(11) \times 10^{-3}\ e^2\ \mathrm{fm}^2$ previously measured using a bremsstrahlung photon beam [23].

IV. DISCUSSION

In this section, the observed $M1$ and $E1$ strength distributions are compared with theoretical predictions based on shell-model and RPA calculations, respectively. Because the present framework based on the large-scale shell-model calculation, which enables a more detailed comparison with experimental data, was applicable only for the $M1$ strength distribution, the RPA approach was adopted for the $E1$ strength calculation.

A. $M1$ strength

The large-scale shell-model calculations were performed using the code MSHELL [37]. To reduce the amount of computation, the active model space was truncated by considering configurations of $(f_{7/2})^{14-t}(p_{3/2}, f_{5/2}, p_{1/2})^{2+t}$, with $t \leqslant 5$, which were sufficient to obtain reasonable convergence of the calculated $M1$ strength distribution at excitation energies below 10 MeV. The standard effective spin g factor, i.e., $g_s^{\mathrm{eff}} = 0.75 g_s^{\mathrm{free}}$ [38], was used in the calculations. Here, the two different types of effective interactions known as GXPF1J [31] and KB3G [32] were adopted. These interactions have

TABLE I. Parity assignments of the observed resonant states obtained using the azimuthal intensity asymmetry A. Reduced transition probabilities $B(\sigma\lambda)\uparrow$ were calculated using information on ground-state decay widths Γ_0 taken from Ref. [23].

E_x (keV)[a]	Γ_0 (meV)[b]	J^π[c]	A	J^π	$B(E1)\uparrow$ (10^{-3} e^2 fm^2)	$B(M1)\uparrow$ (μ_N^2)
3448.6(2)	78(5)	1^+				0.49(3)
6925.4(3)	750(31)	1^-	−0.66(11)	1^-	6.47(27)	
7066.4(9)	268(28)	1	−0.65(24)	1^-	2.18(23)	
7166.0(7)	175(22)	1^-	0.81(21)	1^+		0.124(16)
7211.1(3)	614(38)	1^+	0.93(9)	1^+		0.425(26)
7249.4(5)	219(34)	1^+	0.92(13)	1^+		0.149(23)
7282.2(7)	266(41)	1	−0.37(22)	1^-	1.97(30)	
7446.2(6)	189(30)	1	−0.78(16)	1^-	1.31(21)	
7467.6(5)	260(55)	1^+	0.93(14)	1^+		0.162(34)
7887.6(7)	396(92)	(1)	0.73(18)	$(1)^+$		0.210(49)
8011.9(6)	547(48)	1	−0.75(26)	1^-	3.05(27)	
8119.6(8)	391(52)	1	0.39(10)	1^+		0.190(25)
8128.7(4)	1526(61)	1^-	−0.80(10)	1^-	8.14(33)	
8219.4(6)	372(58)	1	−0.67(19)	1^-	1.92(30)	
8239.6(5)	3257(81)	1^-	−0.65(7)	1^-	16.69(41)	
8343.3(6)	357(52)	1	−0.51(17)	1^-	1.76(26)	
8536.3(4)	2714(112)	1^-	−0.57(11)	1^-	12.50(52)	
8652.5(8)	403(70)	1	0.55(9)	1^+		0.162(28)
8766.1(8)	649(78)	1	−0.33(19)	1^-	2.76(33)	
8879.3(9)	402(68)	1	0.62(33)	1^+		0.149(25)
8908.9(12)	647(316)	(1^+)	0.65(27)	$(1)^+$		0.24(12)
8963.6(7)	454(82)	1	0.54(22)	1^+		0.164(30)
8988.9(6)	639(72)	1	0.74(32)	1^+		0.229(26)
9107.8(8)	838(78)	$1^{(-)}$	0.55(13)	1^+		0.288(27)
9137.6(5)	844(87)	1^-	−0.41(20)	1^-	3.17(33)	
9156.8(10)	1384(122)	$1^{(-)}$		$1^{(-)}$	5.17(46)	
9287.6(10)	899(81)	1^-	−0.40(19)	1^-	3.22(29)	
9312.2(8)	869(88)	1	0.59(16)	1^+		0.280(28)
9323.7(7)	767(88)	1	−0.47(14)	1^-	2.71(31)	
9385(1)[d]			0.46(22)	+		
9402.0(6)	1305(155)	1	0.44(19)	1^+		0.408(48)
9434.9(23)	313(71)		0.74(37)	+		0.097(22)[e]
9549(1)[d]			−0.19(12)	−		
9554.8(13)	680(119)	1	0.37(11)	1^+		0.203(35)
9604(1)[d]			0.79(38)	+		
9622.9(25)	473(83)	1	0.76(25)	1^+		0.138(24)
9664.7(9)	429(75)		0.87(26)	+		0.123(22)[e]
9732.2(16)[f]	521(152)		−0.59(18)	−	1.62(47)[e]	
9741.7(13)[f]	1618(222)	(1)	−0.59(18)	$(1)^-$	5.02(69)	
9768.2(7)	336(158)		0.72(25)	+		0.094(44)[e]
9802(1)[d]			0.63(34)	+		
9895(5)[g]			−0.49(25)	−		

[a]Energy values taken from Ref. [23].
[b]Γ_0 values taken from Ref. [23].
[c]J^π from Ref. [23].
[d]Observed in this work.
[e]Assumed as dipole transitions.
[f]Observed as a doublet line.
[g]Observed in Ref. [25].

been employed for the description of spin-isospin responses in the pf-shell nuclei around ^{56}Ni [39,40].

Figure 4 compares the experimental $M1$ strength distribution at excitation energies below 10 MeV with the results of the shell-model calculations. As for the gross structure, one can find a strength at 3.5 MeV (data taken from Ref. [23]) which carries a large fraction of the scissors mode [6] as well as a cluster of strengths around 9 MeV. These are reasonably well reproduced by the shell-model calculations with both the GXPF1J and the KB3G effective interactions.

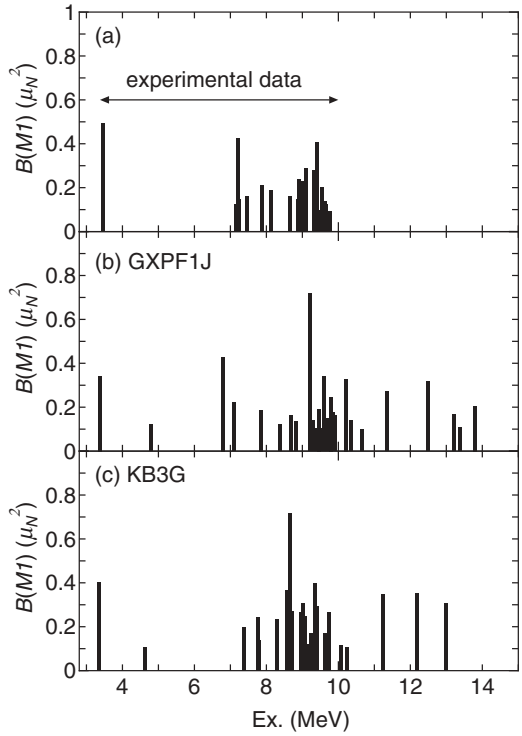

FIG. 4. Experimental $M1$ strength distribution below 10 MeV in ^{56}Fe compared with shell-model calculations obtained using the GXPF1J and KB3G effective interactions. The experimental data at 3.5 MeV are taken from Ref. [23]. Calculated values with $M1$ strength greater than $0.1\mu_N^2$ are shown for direct comparison with the experimental results.

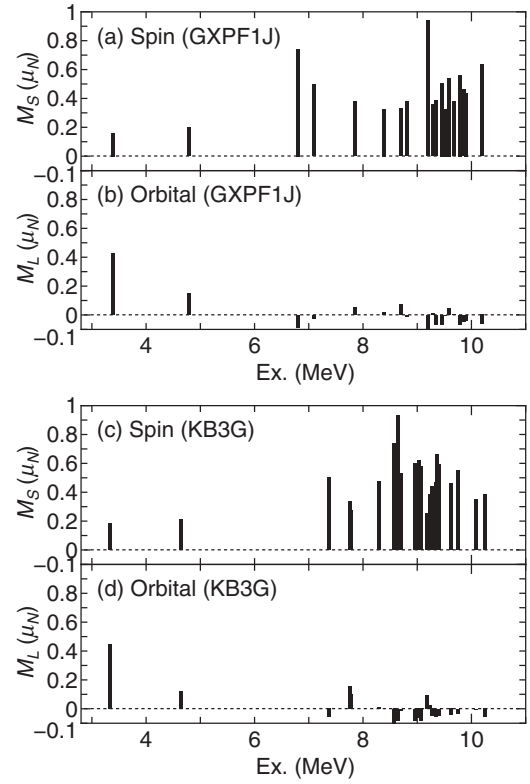

FIG. 5. Spin (M_S) and orbital (M_L) components of the transition matrix elements corresponding to the transitions shown in Figs. 4(b) and 4(c) obtained using the GXPF1J and KB3G effective interactions, respectively. The $M1$ strength is given by $B(M1) = [M_S + M_L]^2$.

The total $M1$ strengths at excitation energies between 6 and 10 MeV are 6.2 and 6.7 μ_N^2 for the GXPF1J and KB3G interactions, respectively. If the calculated strengths greater than $0.1\mu_N^2$, which matches the experimental sensitivity limit, are used, the corresponding summed $M1$ strengths turn out to be $3.6\mu_N^2$ and $5.0\mu_N^2$ for the GXPF1J and KB3G interactions, respectively. The result with the GXPF1J interaction is closer to the experimental value of $\Sigma B(M1)\uparrow = 3.52(17)\mu_N^2$.

In a previous study, a microscopic quasiparticle phonon model (QPM) was used to calculate the 1^+ excited states in ^{56}Fe by including all one-phonon 1^+ configurations up to 15 MeV in the wave function [23]. The two-phonon configurations with excitation energies below 14 MeV and the three-phonon configurations were also included in the model space. The calculated $M1$ strength was centered at 8.8 MeV and tailed off to about 8 and 10 MeV. The $M1$ strength contained in this energy region (8–10 MeV) was obtained to be $9.9\mu_N^2$, while the total $M1$ strength from 4 to 10 MeV was found to be $10.2\mu_N^2$, greater than the values of 6.2 and $6.7\mu_N^2$ obtained by the present shell-model calculations. There was more fragmentation in the experiment than in the theoretical QPM calculation. It was found that deformation of ^{56}Fe could influence the calculated strength and distribution [23].

Figures 5(a)–5(d) show the spin (M_S) and orbital (M_L) components of the transition matrix elements (given by $B(M1) = [M_S + M_L]^2$) corresponding to the transitions presented in Figs. 4(b) and 4(c). The prominent peak at 3.5 MeV and several small strengths below $E_x \approx 7$ MeV are mostly due to the orbital contribution of the $M1$ operator, whereas the strengths above $E_x \approx 7$ MeV are dominated by the spin contribution. A similar result is obtained from the previous calculation with the KB3G interaction [6]. The orbital dominance in these low-lying states and their collective character were pointed out in a previous study based on a shell-model calculation in a more restricted model space [41].

As stated above, the gross structure of the $M1$ strength distribution is similar in the results obtained with the GXPF1J and KB3G interactions. However, the details of the spin-dominant part shown in Figs. 5(a) and 5(c) represent different distributions. To quantify the $M1$ strength distribution, the centroid energy E_c and its variance σ_{E_c}, defined by the following equations, were examined in the energy range between 6 and 10 MeV:

$$E_c = \Sigma\{E_x \cdot B(M1)\uparrow\}/\Sigma B(M1)\uparrow, \quad (6)$$

$$\sigma_{E_c} = [\Sigma\{(E_x - E_c)^2 \cdot B(M1)\uparrow\}/\Sigma B(M1)\uparrow]^{1/2}. \quad (7)$$

In the evaluation, we used the transitions with $M1$ strengths greater than $0.1\mu_N^2$ for direct comparison with experimental values. The results are summarized in Table II. The centroid energies for both the GXPF1J and KB3G interactions give $E_c = 8.8$ MeV, which is close to the experimental value of 8.6 MeV. On the other hand, the $M1$ strength distribution

TABLE II. Comparison of the total $M1$ strengths $\Sigma B(M1)\uparrow$, the energy centroid E_c, and the variance σ_{E_c} in the energy range between 6 and 10 MeV.

Shell model interactions	$\Sigma B(M1)\uparrow$ (units of μ_N^2)	E_c (MeV)	σ_{E_c} (MeV)
GXPF1J[a]	3.6	8.8	1.0
KB3G[a]	5.0	8.8	0.58
Experiment	3.52(17)	8.6	0.86

[a]Calculated values with $M1$ strength greater than 0.1 μ_N^2 are used for the evaluation.

is broader for the GXPF1J interaction than for the KB3G interaction. The GXPF1J interaction also predicts a higher centroid energy and broader width for the Gamow-Teller (GT) strength distribution in ^{56}Fe and ^{56}Ni than the KB3G interaction [40]. The broader GT strength distribution is supported by a recent measurement on ^{56}Ni [42]. A relatively large strength ($\approx 0.4\mu_N^2$) at 6.8 MeV obtained using the GXPF1J interaction is apparent in Fig. 4(b). This strength is dominated by the $f_{7/2} \rightarrow f_{7/2}$ transitions caused by destructive interference between protons and neutrons. Because the contributions of the protons and neutrons to the $M1$ matrix elements are similar in magnitude for the KB3G interaction, the corresponding $M1$ strength is missing (or rather small), as shown in Fig. 4(c). This is in contrast to the $f_{7/2} \rightarrow f_{5/2}$ spin-flip transitions dominated at excitation energies above 8 MeV, where protons and neutrons contribute additively to the $M1$ operator. Thus, the details of the $M1$ strength distribution depend on the choice of the effective interaction and can be tested by comparison with experimental observations.

Finally, the calculations with both the GXPF1J and KB3G interactions predict several $M1$ strengths with $\approx 0.3\mu_N^2$ at excitation energies above 10 MeV. It would be worthwhile to extend the photon-scattering experiments to higher excitation energies up to the neutron separation energy (11.2 MeV) of ^{56}Fe.

B. $E1$ strength

The summed $E1$ strength at $E_x = 6.9$–9.8 MeV in ^{56}Fe is determined to be $\Sigma B(E1)\uparrow = 78.0(15) \times 10^{-3}\ e^2\ \mathrm{fm}^2$, corresponding to 0.317(6)% of the energy-weighted TRK sum rule value. Almost half of this $E1$ strength is carried by three transitions at 8129, 8240, and 8536 keV, which form a small $E1$ concentration below the neutron separation energy.

To provide a theoretical basis for the identified $E1$ strength, we have performed microscopic calculations within the framework of the RPA by using a revised version of the RPA code described in Ref. [33]. The self-consistent RPA equation was solved by the conventional diagonalization method. The representation of the three-dimensional Cartesian grids was adopted within a sphere of radius $R_{\mathrm{box}} = 15$ fm. We used the Skyrme functional of the SkM* parameter set [43], which has been widely used to describe the properties of deformed nuclei.

The RPA calculation yields two $E1$ modes, $K = 0$ and $K = 1$, corresponding to oscillations along two different axes in prolate deformed nuclei. The $K = 0$ ($K = 1$) mode is dominant at excitation energies below (above) 11 MeV. The calculated summed $E1$ strength and the summed energy-weighted $E1$ strength below 10 MeV are 76.2 $\times 10^{-3}\ e^2$ fm^2 and 680 $\times 10^{-3}\ e^2$ fm^2 MeV (0.328% of the TRK value), respectively, by taking only the $E1$ strengths greater than $1 \times 10^{-3}\ e^2$ fm^2, i.e., the sensitivity limit in the experiment. The calculated values agree with the observed values, as compared in Table III.

TABLE III. Comparison of the experimental data with RPA calculations for the $E1$ strengths in ^{56}Fe at excitation energies below 10 MeV. The summed strength $\Sigma B(E1)\uparrow$, energy-weighted strength $\Sigma E_x \cdot B(E1)\uparrow$, and its value relative to the Thomas-Reiche-Kuhn (TRK) sum rule value are summarized.

	$\Sigma B(E1)\uparrow$ ($10^{-3}\ e^2$ fm^2)	$\Sigma E_x \cdot B(E1)\uparrow$ ($10^{-3}\ e^2$ fm^2 MeV)	$\Sigma E_x \cdot B(E1)\uparrow$ (% TRK)
RPA[a]	76.2	680	0.328
Experiment	78.0(15)	654(13)	0.317(6)

[a]Calculated values with $E1$ strength greater than $1 \times 10^{-3}\ e^2$ fm^2 are used for the evaluation.

In a previous QPM calculation, a total $E1$ strength of 110 $\times 10^{-3}\ e^2$ fm^2 between 5 and 10 MeV was obtained by including configurations up to the coupling of three phonons [23]. Because one-phonon configurations up to an energy of 25 MeV were taken into account, the influence of the GDR on low-lying 1^- states was well incorporated, and therefore, the renormalization of effective charges corresponding to core-polarization effects was not needed in the $E1$ operator [15]. The value obtained from the QPM calculation is greater than that obtained from the present RPA calculation.

In unstable neutron-rich nuclei such as ^{68}Ni [14] and Sn isotopes [16,17], a low-energy $E1$ strength of 3%–5% of the TRK value has been observed. The enhanced $E1$ strength might originate from collective skin oscillations of the excess neutrons against the proton-neutron saturated core [7]. No such enhancement is observed in ^{56}Fe. An enhanced $E1$ strength of more than 3% of the TRK value below the excitation energy of 10 MeV is predicted theoretically for neutron-rich nuclei with neutron numbers of $N \geqslant 52$ in the iron region [44].

V. CONCLUSION

In conclusion, photon-scattering experiments on ^{56}Fe were performed with a quasimonochromatic, linearly polarized photon beam. Although 53 dipole states at excitation energies below 10 MeV in ^{56}Fe have been observed in a previous experiment using a bremsstrahlung photon beam, parity quantum numbers have been determined for only 16 excited levels. From the present high-resolution measurements, the parity quantum numbers were determined for 33 dipole states previously known. The summed strengths of $\Sigma B(M1)\uparrow = 3.52(17)\mu_N^2$ and $\Sigma B(E1)\uparrow = 78.0(15) \times 10^{-3}\ e^2$ fm^2 at excitation energies between 7 and 10 MeV were determined. These values are greater than those obtained in a previous photon-scattering experiment with a bremsstrahlung photon beam. The measured $M1$ strengths were compared with shell-model predictions using the GXPF1J and KB3G effective interactions. Both

calculations reproduced the gross structure of the measured $M1$ strength distribution. However, the calculated $M1$ strength distribution with the GXPF1J interaction was broader than that with the KB3G interaction. The summed $E1$ strength of $78.0(15) \times 10^{-3}$ e^2 fm^2 corresponds to 0.317(6)% of the TRK sum value. These values can be reproduced by the RPA calculation with the Skyrme interaction.

ACKNOWLEDGMENTS

This work was supported by Grant-in-Aid for Scientific Research (B) No. 18340071, Grant-in-Aid for Scientific Research (C) No. 19540262, Grant No. 20540300 from JSPS, and Grant-in-Aid for Scientific Research on Innovative Areas No. 24105008 from MEXT.

[1] A. Richter, Prog. Part. Nucl. Phys. **34**, 261 (1995).
[2] K. Langanke, G. Martínez-Pinedo, P. von Neumann-Cosel, and A. Richter, Phys. Rev. Lett. **93**, 202501 (2004).
[3] A. Bohr and B. R. Mottelson, *Nuclear Structure* (Benjamin, New York, 1975).
[4] D. I. Sober, B. C. Metsch, W. Knüpfer, G. Eulenberg, G. Küchler, A. Richter, E. Spamer, and W. Steffen, Phys. Rev. C **31**, 2054 (1985).
[5] W. Mettner, A. Richter, W. Stock, B. C. Metsch, and A. G. M. van Hees, Nucl. Phys. A **473**, 160 (1987).
[6] R. W. Fearick, G. Hartung, K. Langanke, G. Martínez-Pinedo, P. von Neumann-Cosel, and A. Richter, Nucl. Phys. A **727**, 41 (2003).
[7] N. Paar, D. Vretenar, E. Khan, and G. Coló, Rep. Prog. Phys. **70**, 691 (2007).
[8] S. Goriely and E. Khan, Nucl. Phys. A **706**, 217 (2002).
[9] J. Piekarewicz, Phys. Rev. C **73**, 044325 (2006).
[10] B. A. Brown, Phys. Rev. Lett. **85**, 5296 (2000).
[11] A. Leistenschneider *et al.*, Phys. Rev. Lett. **86**, 5442 (2001).
[12] E. Tryggestad, T. Baumann, P. Heckman, M. Thoennessen, T. Aumann, D. Bazin, Y. Blumenfeld, J. R. Beene, T. A. Lewis, D. C. Radford, D. Shapira, R. L. Varner, M. Chartier, M. L. Halbert, and J. F. Liang, Phys. Rev. C **67**, 064309 (2003).
[13] T. Hartmann, M. Babilon, S. Kamerdzhiev, E. Litvinova, D. Savran, S. Volz, and A. Zilges, Phys. Rev. Lett. **93**, 192501 (2004).
[14] O. Wieland *et al.*, Phys. Rev. Lett. **102**, 092502 (2009).
[15] K. Govaert, F. Bauwens, J. Bryssinck, D. De Frenne, E. Jacobs, W. Mondelaers, L. Govor, and V. Yu. Ponomarev, Phys. Rev. C **57**, 2229 (1998).
[16] P. Adrich *et al.*, Phys. Rev. Lett. **95**, 132501 (2005).
[17] A. Klimkiewicz *et al.*, Phys. Rev. C **76**, 051603(R) (2007).
[18] N. Ryezayeva, T. Hartmann, Y. Kalmykov, H. Lenske, P. von Neumann-Cosel, V. Yu. Ponomarev, A. Richter, A. Shevchenko, S. Volz, and J. Wambach, Phys. Rev. Lett. **89**, 272502 (2002).
[19] J. Enders, P. von Brentano, J. Eberth, A. Fitzler, C. Fransen, R.-D. Herzberg, H. Kaiser, L. Kaubler, P. von Neumann-Cosel, N. Pietralla, V. Yu. Ponomarev, A. Richter, R. Schwengner, and I. Wiedenhöver, Nucl. Phys. A **724**, 243 (2003).
[20] R.-D. Herzberg *et al.*, Phys. Lett. B **390**, 49 (1997).
[21] D. Savran, M. Fritzsche, J. Hasper, K. Lindenberg, S. Müller, V. Yu. Ponomarev, K. Sonnabend, and A. Zilges, Phys. Rev. Lett. **100**, 232501 (2008).
[22] A. P. Tonchev, S. L. Hammond, J. H. Kelley, E. Kwan, H. Lenske, G. Rusev, W. Tornow, and N. Tsoneva, Phys. Rev. Lett. **104**, 072501 (2010).
[23] F. Bauwens, J. Bryssinck, D. De Frenne, K. Govaert, L. Govor, M. Hagemann, J. Heyse, E. Jacobs, W. Mondelaers, and V. Y. Ponomarev, Phys. Rev. C **62**, 024302 (2000).
[24] N. Kumagai, T. Ishimatsu, E. Tanaka, K. Kageyama, and G. Isoyama, Nucl. Phys. A **329**, 205 (1979).
[25] T. Chapuran, R. Starr, R. Vodhanel, and M. K. Brussel, Phys. Rev. C **30**, 54 (1984).
[26] K. Govaert, W. Mondelaers, E. Jacobs, D. De Frenne, K. Persyn, S. Pomme, M.-L. Yoneama, S. Lindenstruth, K. Huber, A. Jung, B. Starck, R. Stock, C. Wesselborg, R.-D. Heil, U. Kneissl, and H. H. Pitz, Nucl. Instrum. Methods Phys. Res., Sect. A **337**, 265 (1994).
[27] U. Kneissl, H. H. Pitz, and A. Zilges, Prog. Part. Nucl. Phys. **37**, 349 (1996).
[28] N. Pietralla, Z. Berant, V. N. Litvinenko, S. Hartman, F. F. Mikhailov, I. V. Pinayev, G. Swift, M. W. Ahmed, J. H. Kelley, S. O. Nelson, R. Prior, K. Sabourov, A. P. Tonchev, and H. R. Weller, Phys. Rev. Lett. **88**, 012502 (2001).
[29] T. Shizuma, T. Hayakawa, H. Ohgaki, H. Toyokawa, T. Komatsubara, N. Kikuzawa, A. Tamii, and H. Nakada, Phys. Rev. C **78**, 061303(R) (2008).
[30] M. Honma, T. Otsuka, B. A. Brown, and T. Mizusaki, Phys. Rev. C **69**, 034335 (2004).
[31] M. Honma, T. Otsuka, T. Mizusaki, M. Hjorth-Jensen, and B. A. Brown, J. Phys. Conf. Ser. **20**, 7 (2005).
[32] A. Poves, J. Sánchez-Solano, E. Caurier, and F. Nowacki, Nucl. Phys. A **694**, 157 (2001).
[33] T. Inakura, H. Imagawa, Y. Hashimoto, S. Mizutori, M. Yamagami, and K. Matsuyanagi, Nucl. Phys. A **768**, 61 (2006).
[34] H. Ohgaki, S. Sugiyama, T. Yamazaki, T. Mikado, M. Chiwaki, K. Yamada, R. Suzuki, T. Noguchi, and T. Tomimasu, IEEE Trans. Nucl. Sci. **38**, 386 (1991).
[35] W. R. Nelson, H. Hirayama, and W. O. Roger, SLAC National Accelerator Laboratory, Report No. SLAC-R-265, 1985 (unpublished).
[36] L. W. Fagg and S. S. Hanna, Rev. Mod. Phys. **31**, 711 (1959).
[37] T. Mizusaki, RIKEN Accel. Prog. Rep. **33**, 14 (2000).
[38] P. von Neumann-Cosel, A. Poves, J. Retamosa, and A. Richter, Phys. Lett. B **443**, 1 (1998).
[39] T. Suzuki, M. Honma, K. Higashiyama, T. Yoshida, T. Kajino, T. Otsuka, H. Umeda, and K. Nomoto, Phys. Rev. C **79**, 061603(R) (2009).
[40] T. Suzuki, M. Honma, H. Mao, T. Otsuka, and T. Kajino, Phys. Rev. C **83**, 044619 (2011).
[41] H. Nakada and T. Otsuka, Phys. Rev. C **55**, 2418 (1997).
[42] M. Sasano *et al.*, Phys. Rev. Lett. **107**, 202501 (2011).
[43] J. Bartel, P. Quentin, M. Brack, C. Guet, and H. B. Håkansson, Nucl. Phys. A **386**, 79 (1982).
[44] T. Inakura, T. Nakatsukasa, and K. Yabana, Phys. Rev. C **84**, 021302(R) (2011).